Discrete representations for Marchenko imaging of imperfectly sampled data

Wapenaar, Kees; van IJsseldijk, Johno

DOI
10.1190/geo2019-0407.1

Publication date
2020

Document Version
Accepted author manuscript

Published in
Geophysics

Discrete representations for Marchenko imaging of imperfectly sampled data

Kees Wapenaar and Johno van IJsseldijk

Delft University of Technology, Department of Geoscience and Engineering, Delft, The Netherlands

(Dated: November 15, 2019)

ABSTRACT

Marchenko imaging is based on integral representations for focusing functions and Green's functions. In practice the integrals are replaced by finite summations. This works well for regularly sampled data, but the quality of the results degrade in case of imperfect sampling. Here we introduce discrete representations that account for imperfect sampling of the sources (or, via reciprocity, of the receivers). These representations contain point-spread functions which explain the blurring of the focusing functions and Green's functions due to the imperfect sampling. Deblurring the focusing functions and Green's functions involves multidimensional deconvolution for the point-spread functions. The discrete representations form the basis for modifying Marchenko imaging to account for imperfectly sampled data, which is important for field data applications.

INTRODUCTION

Marchenko imaging is based on integral representations for Green's functions with virtual sources and/or receivers in the subsurface (Broggini and Snieder, 2012; Slob et al., 2014; Wapenaar et al., 2014). In practice the integrals are replaced by finite summations over the available sources (or, via reciprocity, over the available receivers). This works well for regularly sampled sources (or receivers) obeying the Nyquist criterion, on a large enough grid. Most authors that use the Marchenko method tacitly assume that these conditions are fulfilled, however, some authors have investigated the effects of imperfect sampling. Peng et al. (2019) numerically evaluate the effect of downsampling the sources and/or receivers in a regular way. Staring and Wapenaar (2019) numerically investigate the effects of missing near offsets, limited crossline aperture and undersampling in the crossline direction on 3D Marchenko imaging. Apart from

evaluating the effects of imperfect sampling, one would also like to compensate for them. Ravasi (2017) and Haindl et al. (2018) consider the situation of irregularly sampled sources and well-sampled receivers. Using reciprocity, they reformulate the representation integrals along the well-sampled receivers and propose a sparse inversion method to compensate for the source irregularity.

Ultimately, one would like to compensate for imperfect sampling of the sources as well as the receivers. This paper aims to make a first step in that direction by reformulating the integral representations in terms of discrete finite summations over imperfectly sampled sources. This is akin to reformulating the representations underlying seismic interferometry for irregular source distributions. For seismic interferometry the approach is as follows. The classical correlation integral representation is replaced by an implicit convolution integral representation, which is subsequently inverted by multidimensional deconvolution (MDD; Wapenaar et al., 2011). The point-spread function (PSF) plays a central role in this approach (Van der Neut and Wapenaar, 2015). This approach is not straightforwardly adapted for Marchenko imaging, because this method is based on a combination of convolution and correlation integral representations. Following a different route, we derive discrete representations for Marchenko imaging, which include PSF's. We illustrate these representations with numerical examples. These representations form the basis for modified Marchenko imaging of imperfectly sampled data, which is subject of ongoing research.

INTEGRAL REPRESENTATIONS

We consider an inhomogeneous lossless acoustic medium bounded by acquisition surface $\mathbb{S}_0$ (Figure 1(a)). We assume this surface is reflection free and the half-space above it is homogeneous. The reflection response at this surface is given by $R(\mathbf{x}_R, \mathbf{x}_S, t)$, where $\mathbf{x}_S$ and $\mathbf{x}_R$ denote

the source and receiver positions, respectively, and t denotes time. Let us define a virtual receiver position $\mathbf{x}_A$ inside the inhomogeneous medium. Green's functions from the surface $\mathbb{S}_0$ to this virtual receiver are given by $G^+(\mathbf{x}_A, \mathbf{x}_R, t)$ and $G^-(\mathbf{x}_A, \mathbf{x}_R, t)$, where the superscripts + and − denote downward and upward propagation, respectively, at $\mathbf{x}_A$. Next, we define a horizontal surface $\mathbb{S}_A$ at the depth of the virtual receiver. We consider a truncated version of the medium, which is identical to the actual medium above $\mathbb{S}_A$ and homogeneous below it (Figure 1(b)). At $\mathbb{S}_0$ we introduce a downgoing focusing function $f_1^+(\mathbf{x}_S, \mathbf{x}_A, t)$ which, when emitted from all $\mathbf{x}_S$ at $\mathbb{S}_0$ into the truncated medium, focuses at $\mathbf{x}_A$. Its upgoing response at $\mathbb{S}_0$ is denoted by $f_1^-(\mathbf{x}_R, \mathbf{x}_A, t)$.

All these quantities are related via the following integral representations

$$G^-(\mathbf{x}_A, \mathbf{x}_R, t) + f_1^-(\mathbf{x}_R, \mathbf{x}_A, t) = \int_{\mathbb{S}_0} R(\mathbf{x}_R, \mathbf{x}_S, t) * f_1^+(\mathbf{x}_S, \mathbf{x}_A, t) \mathrm{d}\mathbf{x}_S, \tag{1}$$

$$G^+(\mathbf{x}_A, \mathbf{x}_R, t) - f_1^+(\mathbf{x}_R, \mathbf{x}_A, -t) = -\int_{\mathbb{S}_0} R(\mathbf{x}_R, \mathbf{x}_S, t) * f_1^-(\mathbf{x}_S, \mathbf{x}_A, -t) \mathrm{d}\mathbf{x}_S, \tag{2}$$

where the asterisk ($*$) denotes temporal convolution. These representations hold for flux-normalised as well as pressure-normalised wave fields (Wapenaar et al., 2014).

We illustrate these representations with a 2D numerical example, assuming for the moment that the source positions $\mathbf{x}_S$ are regularly distributed along $\mathbb{S}_0$. For simplicity we consider a horizontally layered medium, of which the propagation velocity and mass density as a function of depth are shown in Figure 2. We define $\mathbb{S}_0$ at $x_3 = 0$ m and $\mathbb{S}_A$ at $x_3 = 1000$ m. We numerically model the reflection response at $\mathbb{S}_0$ and convolve it with a Ricker wavelet with a central frequency of 25 Hz. Also the focusing functions are numerically modeled (since the aim

of this paper is to investigate representations rather than the performance of the Marchenko method). We evaluate the integrals in the right-hand sides of equations 1 and 2 for a fixed receiver position ($x_{1,R} = 0$), using regular source sampling ($\Delta x_{1,S} = 5$ m, nr. of sources is 601). The results are shown in Figures 3(a) and (b), respectively. The red dashed lines separate the retrieved focusing functions from the Green's functions at the left-hand sides of equations 1 and 2 (except for the first event below the red line in Figure 3(b), which belongs to the focusing function and the Green's function, as indicated by the arrows).

In practice, the right-hand sides of equations 1 and 2 are approximated by summations, according to

$$\sum_i R(\mathbf{x}_R, \mathbf{x}_S^{(i)}, t) * f_1^+(\mathbf{x}_S^{(i)}, \mathbf{x}_A, t) * S(t) \tag{3}$$

and

$$-\sum_i R(\mathbf{x}_R, \mathbf{x}_S^{(i)}, t) * f_1^-(\mathbf{x}_S^{(i)}, \mathbf{x}_A, -t) * S(t), \tag{4}$$

respectively, with $S(t)$ the source wavelet. Assuming the source position $\mathbf{x}_S^{(i)}$ is imperfectly sampled, these approximations have an effect on the retrieved focusing functions and Green's functions. We illustrate this with a numerical example. Figure 4 shows an irregular distribution of source positions $\mathbf{x}_S^{(i)}$ along $\mathbb{S}_0$ (average $\Delta x_{1,S} = 16.7$ m, nr. of samples is 181). We evaluate equations 3 and 4, using resampled versions of the reflection response and focusing functions of the previous example (the sources are resampled; the receiver position is again fixed at $x_{1,R} = 0$). The results, which are shown in Figures 5(a) and (b), respectively, are blurred versions of those in Figure 3. This blurring can be quantified by PSF's, which are introduced in the next section.

POINT-SPREAD FUNCTIONS

The focusing function f_1^+ is defined as the inverse of the transmission response between $\mathbb{S}_0$ and $\mathbb{S}_A$. This is quantified as follows

$$\delta(\mathbf{x}'_{\mathrm{H},A} - \mathbf{x}_{\mathrm{H},A})\delta(t) = \int_{\mathbb{S}_0} T(\mathbf{x}'_A, \mathbf{x}_S, t) * f_1^+(\mathbf{x}_S, \mathbf{x}_A, t)\mathrm{d}\mathbf{x}_S, \tag{5}$$

with $\mathbf{x}'_A$ and $\mathbf{x}_A$ at $\mathbb{S}_A$, and $\mathbf{x}'_{\mathrm{H},A}$ and $\mathbf{x}_{\mathrm{H},A}$ denoting the horizontal coordinates of $\mathbf{x}'_A$ and $\mathbf{x}_A$, respectively. Here T stands for the flux-normalised transmission response or for a modified version $\mathcal{T}$ of the pressure-normalised transmission response (Wapenaar et al., 2014). For the case of imperfect sampling, the discretised band-limited version of equation 5 reads

$$\Gamma^+(\mathbf{x}'_A, \mathbf{x}_A, t) = \sum_i T(\mathbf{x}'_A, \mathbf{x}_S^{(i)}, t) * f_1^+(\mathbf{x}_S^{(i)}, \mathbf{x}_A, t) * S(t), \tag{6}$$

where $\Gamma^+(\mathbf{x}'_A, \mathbf{x}_A, t)$ is a PSF. It is illustrated in Figure 6(a) (obtained from the numerically modelled f_1^+ and T), for the same irregular source distribution that was used in the example in Figure 5. In the next section we show that this PSF explains the blurring in Figure 5(a). However, it does not explain the blurring in Figure 5(b). For this we need a second PSF, which we discuss now.

Analogous to equation 5, we define a quantity Y as the inverse of f_1^- as follows

$$\delta(\mathbf{x}'_{\mathrm{H},A} - \mathbf{x}_{\mathrm{H},A})\delta(t) = \int_{\mathbb{S}_0} Y(\mathbf{x}'_A, \mathbf{x}_S, t) * f_1^-(\mathbf{x}_S, \mathbf{x}_A, -t)\mathrm{d}\mathbf{x}_S. \tag{7}$$

In the following we tacitly assume that Y exists, but we remark that, since f_1^- is a reflection response, inversion of equation 7 for Y may not always be stable. Analogous to equation 6, we define a PSF for the case of imperfect sampling as follows

$$\Gamma^-(\mathbf{x}'_A, \mathbf{x}_A, t) = \sum_i Y(\mathbf{x}'_A, \mathbf{x}_S^{(i)}, t) * f_1^-(\mathbf{x}_S^{(i)}, \mathbf{x}_A, -t) * S(t), \tag{8}$$

which is illustrated in Figure 6(b) (obtained from the numerically modelled f_1^- and Y).

DISCRETE REPRESENTATIONS

We use the PSF's introduced in the previous section to transform the integral representations of equations 1 and 2 into discrete representations. We start by applying the operation $\int_{\mathbb{S}_A}\{\cdot\} * \Gamma^+(\mathbf{x}'_A, \mathbf{x}_A, t)\mathrm{d}\mathbf{x}'_A$ to both sides of equation 1 (with $\mathbf{x}_A$ replaced by $\mathbf{x}'_A$). For the terms on the left-hand side we define the blurred functions $\hat{G}^-$ and $\hat{f}_1^-$, according to

$$\hat{G}^-(\mathbf{x}_A, \mathbf{x}_R, t) = \int_{\mathbb{S}_A} G^-(\mathbf{x}'_A, \mathbf{x}_R, t) * \Gamma^+(\mathbf{x}'_A, \mathbf{x}_A, t)\mathrm{d}\mathbf{x}'_A, \tag{9}$$

$$\hat{f}_1^-(\mathbf{x}_R, \mathbf{x}_A, t) = \int_{\mathbb{S}_A} f_1^-(\mathbf{x}_R, \mathbf{x}'_A, t) * \Gamma^+(\mathbf{x}'_A, \mathbf{x}_A, t)\mathrm{d}\mathbf{x}'_A. \tag{10}$$

Applying the same operation to the right-hand side of equation 1, substituting equation 6 and interchanging the order of summation over $\mathbf{x}_S^{(i)}$ and integration along $\mathbb{S}_A$, we obtain

$$\sum_i \int_{\mathbb{S}_0} R(\mathbf{x}_R, \mathbf{x}_S, t) * f_1^+(\mathbf{x}_S^{(i)}, \mathbf{x}_A, t) * S(t) \\ * \int_{\mathbb{S}_A} f_1^+(\mathbf{x}_S, \mathbf{x}'_A, t) * T(\mathbf{x}'_A, \mathbf{x}_S^{(i)}, t) \mathrm{d}\mathbf{x}'_A \mathrm{d}\mathbf{x}_S. \tag{11}$$

Since T and f_1^+ are each other's inverse, the integral along $\mathbb{S}_A$ yields $\delta(\mathbf{x}_{\mathrm{H},S} - \mathbf{x}_{\mathrm{H},S}^{(i)})\delta(t)$, where $\mathbf{x}_{\mathrm{H},S}$ and $\mathbf{x}_{\mathrm{H},S}^{(i)}$ denote the horizontal coordinates of $\mathbf{x}_S$ and $\mathbf{x}_S^{(i)}$, respectively. Using the sift-property of this delta function in the integral along $\mathbb{S}_0$, what remains of equation 11 is a summation over $\mathbf{x}_S^{(i)}$, precisely as formulated in equation 3. Combining the results we thus obtain

$$\hat{G}^-(\mathbf{x}_A, \mathbf{x}_R, t) + \hat{f}_1^-(\mathbf{x}_R, \mathbf{x}_A, t) = \\ \sum_i R(\mathbf{x}_R, \mathbf{x}_S^{(i)}, t) * f_1^+(\mathbf{x}_S^{(i)}, \mathbf{x}_A, t) * S(t). \tag{12}$$

This discrete representation is the counterpart of the integral representation of equation 1. The right-hand side can be seen as the practical implementation of the integral in equation 1 when the sources $\mathbf{x}_S^{(i)}$ are imperfectly sampled. The left-hand side contains blurred versions of the Green's function and the focusing function. According to equation 9, the receiver of the Green's function is smeared around $\mathbf{x}_A$ by the PSF $\Gamma^+(\mathbf{x}'_A, \mathbf{x}_A, t)$. Similarly, equation 10 quantifies the smearing by the PSF of the focal point of the focusing function around $\mathbf{x}_A$. Hence, the PSF $\Gamma^+(\mathbf{x}'_A, \mathbf{x}_A, t)$ explains the blurring observed in Figure 5(a). We deblur this figure by MDD, i.e., by applying the least-squares inverse of the PSF to $\hat{G}^-(\mathbf{x}_A, \mathbf{x}_R, t) + \hat{f}_1^-(\mathbf{x}_R, \mathbf{x}_A, t)$ (for fixed $\mathbf{x}_R$ and variable $\mathbf{x}_A$). Note that, although the medium is laterally invariant, the PSF is not shift-invariant due to the irregular sampling. Hence, MDD requires a full matrix inversion, similar

as for laterally varying media. The result is shown in Figure 7(a) and accurately matches the ideal result in Figure 3(a). The maximum deviation for the central trace is 2.4 %. At far offsets the amplitudes are somewhat overestimated due to limitations of the MDD method.

Next, we apply the operation $\int_{\mathbb{S}_A}\{\cdot\} * \Gamma^-(\mathbf{x}'_A, \mathbf{x}_A, t)\mathrm{d}\mathbf{x}'_A$ to both sides of equation 2 (with $\mathbf{x}_A$ replaced by $\mathbf{x}'_A$). In a similar way as above we obtain

$$\hat{G}^+(\mathbf{x}_A, \mathbf{x}_R, t) - \hat{f}_1^+(\mathbf{x}_R, \mathbf{x}_A, -t) = \tag{13}$$
$$-\sum_i R(\mathbf{x}_R, \mathbf{x}_S^{(i)}, t) * f_1^-(\mathbf{x}_S^{(i)}, \mathbf{x}_A, -t) * S(t),$$

with

$$\hat{G}^+(\mathbf{x}_A, \mathbf{x}_R, t) = \tag{14}$$
$$\int_{\mathbb{S}_A} G^+(\mathbf{x}'_A, \mathbf{x}_R, t) * \Gamma^-(\mathbf{x}'_A, \mathbf{x}_A, t)\mathrm{d}\mathbf{x}'_A,$$
$$\hat{f}_1^+(\mathbf{x}_R, \mathbf{x}_A, -t) = \tag{15}$$
$$\int_{\mathbb{S}_A} f_1^+(\mathbf{x}_R, \mathbf{x}'_A, -t) * \Gamma^-(\mathbf{x}'_A, \mathbf{x}_A, t)\mathrm{d}\mathbf{x}'_A.$$

Equation 13 is the discrete counterpart of the integral representation of equation 2. The PSF $\Gamma^-(\mathbf{x}'_A, \mathbf{x}_A, t)$ in equations 14 and 15 explains the blurring observed in Figure 5(b). Deblurring this figure by MDD yields the result shown in Figure 7(b) which accurately matches the ideal result in Figure 3(a). The maximum deviation for the central trace is 4.7 %. There are also some small edge effects, probably caused by the quantity Y (introduced in equation 7 as the inverse of f_1^-), which is not unconditionally stable. At far offsets the amplitudes are somewhat underestimated due to our efforts to suppress the aforementioned edge effects.

TOWARDS MARCHENKO IMAGING OF IMPERFECTLY SAMPLED DATA

The discrete representations of equations (12) and (13), with the blurred Green's functions and focusing functions defined in equations (9), (10), (14) and (15), form the basis for a modification of the Marchenko method, which accounts for the effects of imperfect source sampling. We propose an iterative scheme, building on the current Marchenko method, where in each iteration the effect of the PSF is removed by MDD (between the evaluation of the summation and the application of the time window). This requires an initial estimate of the PSF's and an update in each iteration. The initial estimate of the PSF can be obtained from an estimate of the direct arrival of the transmission response and the initial focusing functions. For the situation in which the sources and receivers are both imperfectly sampled and occupy different positions, we envisage an iterative scheme which combines the inversion of the discrete representations (to account for imperfect source sampling) with a sparse inversion method such as proposed by Haindl et al. (2018) (to account for imperfect receiver sampling).

CONCLUSIONS

Current implementations of the Marchenko method do not account for imperfect sampling. We have derived discrete representations as an alternative for the integral representations that underlie the Marchenko method. These discrete representations account for the effects of imperfect source sampling (or, via reciprocity, of imperfect receiver sampling). The Green's functions and focusing functions expressed by these representations are blurred by PSF's, for which we derived explicit expressions.

The discrete representations form the basis for a modification of the Marchenko method, which accounts for the effects of the inherent imperfect sampling of seismic field data. The

development of such a modified Marchenko method is subject of ongoing research.

ACKNOWLEDGMENTS

We thank Christian Reinicke for his help with the numerical examples. We thank the associate editor and reviewers for their constructive comments, which helped to improve the paper. We acknowledge funding from the European Research Council (ERC) under the European Union's Horizon 2020 research and innovation programme (grant agreement No: 742703).

DATA AND MATERIALS AVAILABILITY

Data associated with this research are available and can be obtained by contacting the corresponding author.

REFERENCES

Broggini, F. and R. Snieder, 2012, Connection of scattering principles: a visual and mathematical tour: European Journal of Physics, **33**, 593–613.

Haindl, C. M., F. Broggini, M. Ravasi, and D.-J. van Manen, 2018, Using sparsity to improve the accuracy of Marchenko imaging given imperfect acquisition geometries: 80th Annual International Meeting, EAGE, Extended Abstracts, Th–P9–14.

Peng, H., I. Vasconcelos, Y. Sripanich, and L. Zhang, 2019, On the effects of acquisition sampling on Marchenko-based focusing and primary estimation: 81st Annual International Meeting, EAGE, Extended Abstracts, Th–R08–09.

Ravasi, M., 2017, Rayleigh-Marchenko redatuming for target-oriented, true-amplitude imaging: Geophysics, **82**, no. 6, S439–S452.

Slob, E., K. Wapenaar, F. Broggini, and R. Snieder, 2014, Seismic reflector imaging using internal multiples with Marchenko-type equations: Geophysics, **79**, no. 2, S63–S76.

Staring, M. and K. Wapenaar, 2019, Interbed demultiple using Marchenko redatuming on 3D field data of the Santos Basin: 16th International Congress of the Brazilian Geophysical Society, SBGf, Expanded Abstracts.

Van der Neut, J. and K. Wapenaar, 2015, Point-spread functions for interferometric imaging: Geophysical Prospecting, **63**, 1033–1049.

Wapenaar, K., J. van der Neut, E. Ruigrok, D. Draganov, J. Hunziker, E. Slob, J. Thorbecke, and R. Snieder, 2011, Seismic interferometry by crosscorrelation and by multidimensional deconvolution: a systematic comparison: Geophysical Journal International, **185**, 1335–1364.

Wapenaar, K., J. Thorbecke, J. van der Neut, F. Broggini, E. Slob, and R. Snieder, 2014, Green's function retrieval from reflection data, in absence of a receiver at the virtual source position: Journal of the Acoustical Society of America, **135**, no. 5, 2847–2861.

Captions

Fig 1: (a) Inhomogeneous medium, its reflection response and Green's functions. (b) Truncated medium with focusing functions. In both figures the rays stand for full responses, including all orders of multiple scattering.

Fig 2: Propagation velocity and mass density of a horizontally layered medium as a function of depth.

Fig 3: Evaluation of the integrals in equations 1 and 2, for fixed $\mathbf{x}_R$ at $\mathbb{S}_0$ and variable $\mathbf{x}_A$ along $\mathbb{S}_A$.

Fig 4: Irregular distribution of $\mathbf{x}_S^{(i)}$ along $\mathbb{S}_0$. The black bars denote the positions of the sources.

Fig 5: Evaluation of the irregular summations in equations 3 and 4, for fixed $\mathbf{x}_R$ at $\mathbb{S}_0$ and variable $\mathbf{x}_A$ along $\mathbb{S}_A$. Note to the typesetter: if possible, please place Figures 5 and 7 next to each other.

Fig 6: PSF's, as defined by equations 6 and 8, for fixed $\mathbf{x}'_A$ and variable $\mathbf{x}_A$, both at $\mathbb{S}_A$. These PSF's quantify the blurring in Figures 5(a) and (b), respectively.

Fig 7: Results of deblurring Figures 5(a) and (b) by MDD. Note to the typesetter: if possible, please place Figures 5 and 7 next to each other.

FIGURES

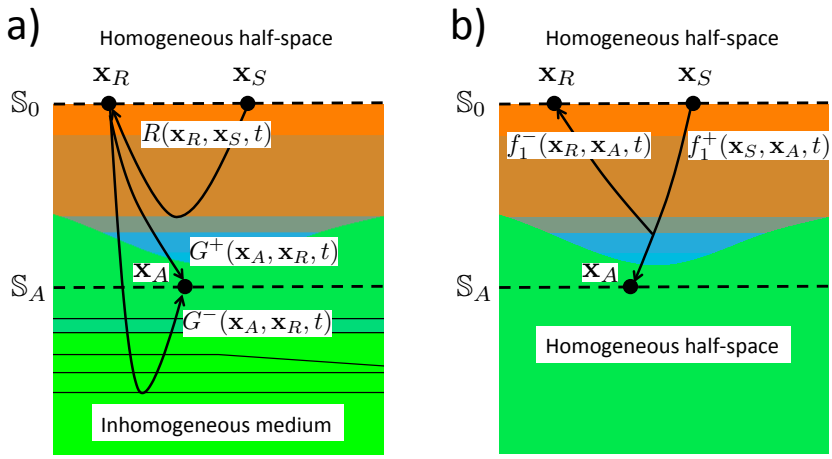

FIG. 1 *(a) Inhomogeneous medium, its reflection response and Green's functions. (b) Truncated medium with focusing functions. In both figures the rays stand for full responses, including all orders of multiple scattering.*

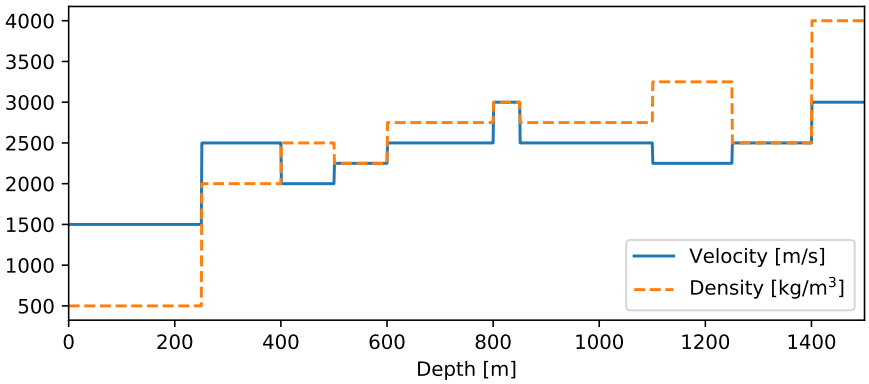

FIG. 2 *Propagation velocity and mass density of a horizontally layered medium as a function of depth.*

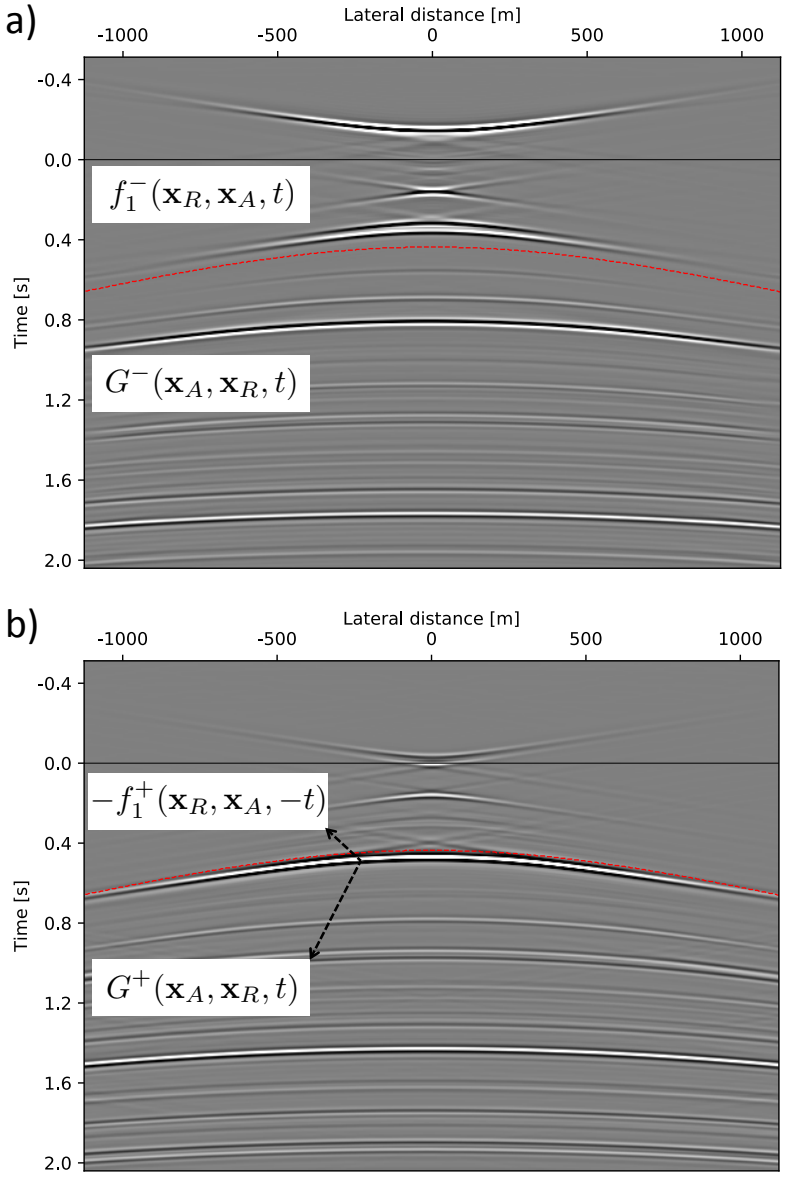

FIG. 3 *Evaluation of the integrals in equations 1 and 2, for fixed* $\mathbf{x}_R$ *at* $\mathbb{S}_0$ *and variable* $\mathbf{x}_A$ *along* $\mathbb{S}_A$.

FIG. 4 *Irregular distribution of* $\mathbf{x}_S^{(i)}$ *along* $\mathbb{S}_0$. *The black bars denote the positions of the sources.*

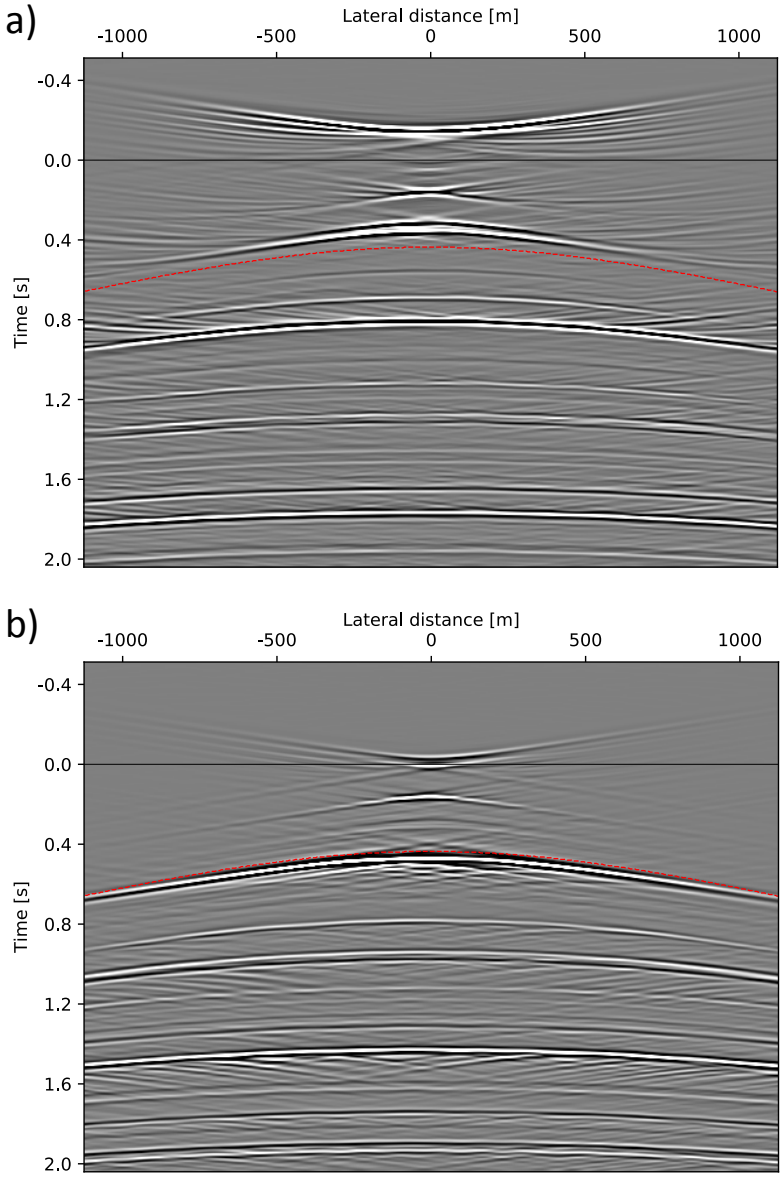

FIG. 5 *Evaluation of the irregular summations in equations 3 and 4, for fixed* $\mathbf{x}_R$ *at* $\mathbb{S}_0$ *and variable* $\mathbf{x}_A$ *along* $\mathbb{S}_A$. *Note to the typesetter: if possible, please place Figures 5 and 7 next to each other.*

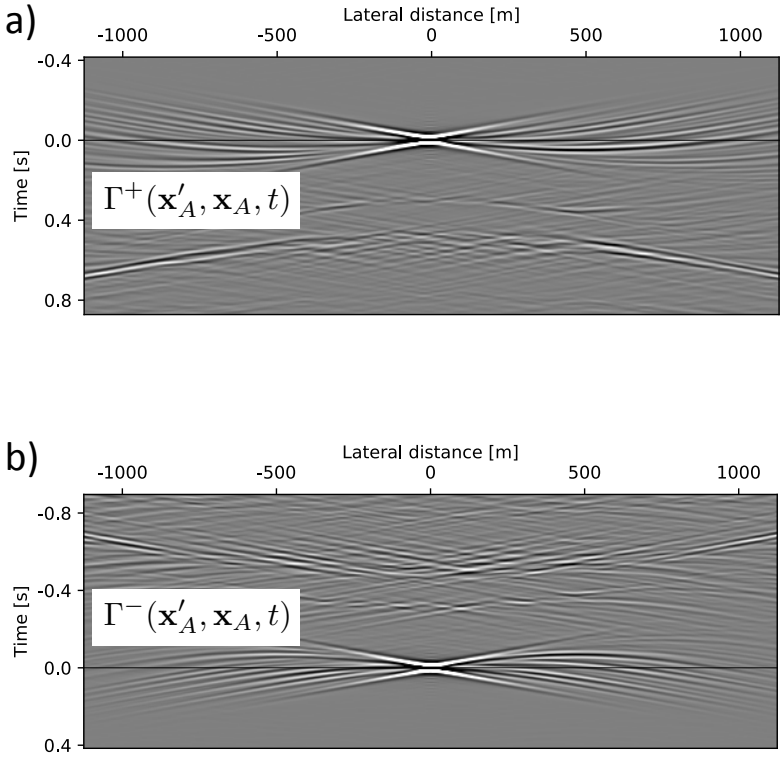

FIG. 6 *PSF's, as defined by equations 6 and 8, for fixed* $\mathbf{x}'_A$ *and variable* $\mathbf{x}_A$*, both at* $\mathbb{S}_A$*. These PSF's quantify the blurring in Figures 5(a) and (b), respectively.*

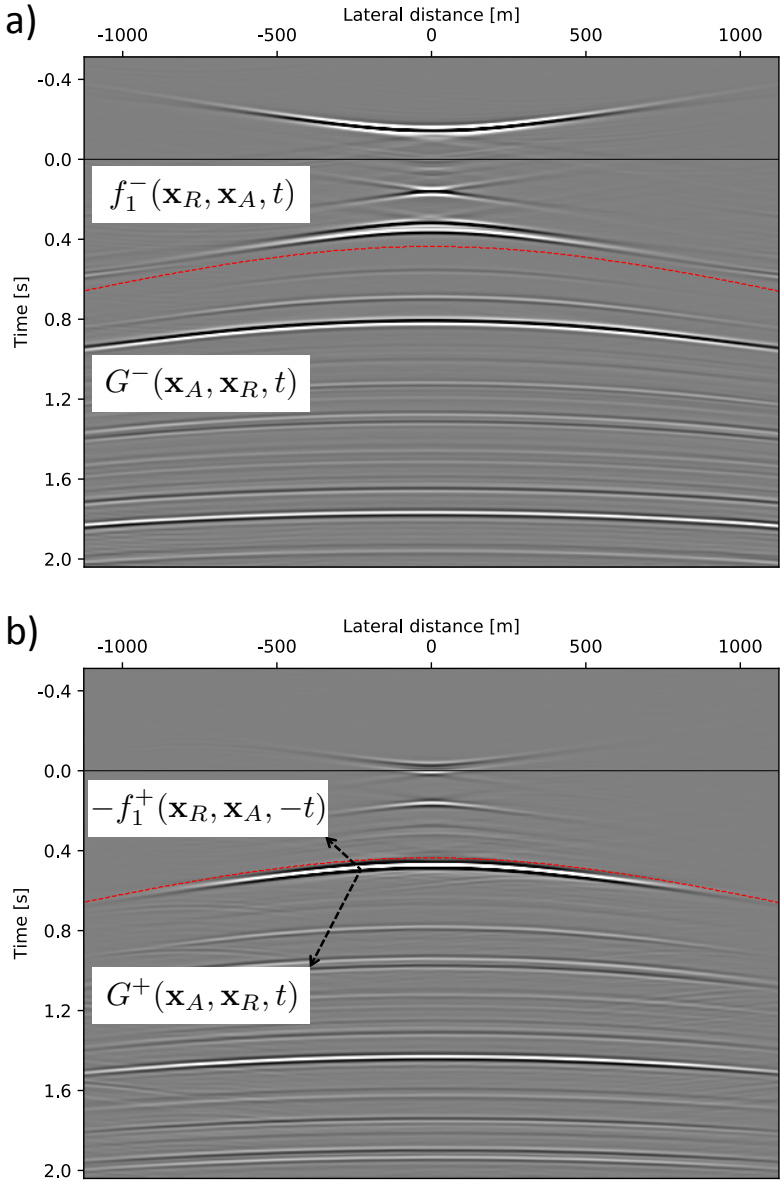

FIG. 7 *Results of deblurring Figures 5(a) and (b) by MDD. Note to the typesetter: if possible, please place Figures 5 and 7 next to each other.*